DEVELOPMENT OF RESVERATROL ENCAPSULATED ZEIN–GUM GHATTI NANOPARTICLES: PHYSICOCHEMICAL PROPERTIES, ANTIOXIDANT CAPACITY AND CYTOTOXICITY AGAINST COLO-205 CELLS

PRATHAMESH AGRAWAL,[*,#] SONALI ARSUL,[*,#] RAKESH DHOLE,[**] HITESHKUMAR CHAUDHARI,[***] AAKASH JETHVA,[****] RAKESHKUMAR DESAI[*****] and LAXMIKANT ZAWAR[*]

[*]*Department of Pharmaceutics, H. R. Patel Institute of Pharmaceutical Education and Research, Shirpur 425405, India*

[**]*Department of Pharmaceutics, KVPs Maharani Ahilyabai Holkar College of Pharmacy, Shirpur-425405, India*

[***]*Department of Quality Assurance, Ingenus Pharmaceuticals NJ LLC, 140 New Dutch Lane, Fairfield, NJ 07004, USA*

[****]*Department of Industrial Pharmacy/Pharmaceutics, The Arnold and Marie Schwartz College of Pharmacy, Long Island, University of Brooklyn, NY, 11201, USA*

[*****]*Department of Regulatory Affairs, RiconPharma LLC, 100 Ford Road, Denville, NJ 07834, USA*

#These authors contributed equally to this work

✉ *Corresponding author: L. R. Zawar, shwet.zawar@gmail.com*

Received June 11, 2026

Resveratrol (RSV), a natural polyphenolic compound with promising anticancer activity, exhibits poor aqueous solubility and low bioavailability, limiting its therapeutic application. This study aimed to develop RSV-loaded zein-gum ghatti nanoparticles (RZGG-NPs) as a targeted drug delivery system for colon cancer therapy. RZGG-NPs were prepared using an antisolvent precipitation method and characterized for physicochemical and biological properties. The nanoparticles were spherical, exhibited a narrow particle size distribution with an average size of 165.4 ± 3.62 nm, and showed high encapsulation efficiency (84.64 ± 0.017%). Differential scanning calorimetry (DSC) and X-ray diffraction (XRD) analyses confirmed successful encapsulation of RSV in an amorphous form. *In vitro* drug release studies demonstrated sustained RSV release from the nanoparticles over an extended period. Antioxidant activity assessed by DPPH radical scavenging assay revealed activity comparable to free RSV. Cytotoxicity studies using COLO-205 colon cancer cells demonstrated significantly anticancer activity of RZGG-NPs. The formulation also exhibited excellent storage stability with minimal changes in particle size and zeta potential, suggesting potential for targeted colon cancer therapy. Overall, RZGG-NPs improved drug delivery performance, sustained release behavior, and therapeutic efficacy, highlighting their suitability for advanced nanomedicine applications in colon cancer.

Keywords: resveratrol, zein, gum ghatti, colon cancer, nanoparticles, antisolvent method, sustained release

INTRODUCTION

Colon cancer is a major worldwide health problem, with more than one million new cases being diagnosed every year, ranking as the third most commonly diagnosed cancer and the fourth most common cause of cancer-related mortality worldwide.[1] The mortality burden of colon cancer is expected to increase substantially by 2040.[2] With the increasing incidence of colon cancer and the limitations associated with conventional chemotherapy, the development of effective oral drug-delivery systems for colon-directed therapy has received considerable attention. According to the International Agency for Research on Cancer (IARC), approximately 1.6 million deaths from colon cancer are projected worldwide by 2040.[2] Population ageing, unhealthy dietary habits, smoking, obesity, and sedentary lifestyles are among the factors associated with the increasing burden of colon cancer.[3]

One of the major challenges associated with cancer therapy is the development of resistance to conventional chemotherapy. Tumour cells may evade apoptosis through several mechanisms, including overexpression of anti-apoptotic genes.[4] Impairment of apoptotic pathways can contribute to tumour progression and resistance to treatment.[5] Therefore, promoting apoptosis in cancer cells represents an important therapeutic strategy for improving anticancer responses while minimizing damage to healthy cells.[6,7]

Resveratrol (RSV) is a naturally occurring polyphenol, predominantly found in grapes and wine, that has attracted considerable interest due to its diverse biological properties, including antioxidant, anti-inflammatory, anti-amyloidogenic, anti-ageing, and antidiabetic activities. RSV has also been associated with protection against metabolic disorders and improvements in glucose homeostasis and physiological endurance.[8] However, its therapeutic application is restricted by poor aqueous solubility, extensive metabolism, and consequently low oral bioavailability.[9] RSV and its glucuronide metabolite, resveratrol-3-*O*-D-glucuronide, have also been reported to influence genes associated with adipogenesis and lipid accumulation, while RSV can inhibit colon cancer cell proliferation through modulation of cyclooxygenase-1 and -2 (COX-1 and COX-2) activity.[10,11]

Several strategies have been investigated to overcome the biopharmaceutical limitations of RSV, including co-administration with compounds capable of modifying its metabolism, structural modification of the RSV molecule, and the development of novel drug-delivery systems.[12,13] Among these approaches, micro- and nanoencapsulation have shown considerable potential for improving the delivery of poorly soluble phenolic compounds, such as RSV.[14] Consequently, nanoparticle-based encapsulation of RSV has been extensively investigated as an approach to modify its physicochemical characteristics and delivery behavior.

The pharmaceutical performance of naturally derived carrier materials is closely related to their physicochemical and technological characteristics. Previous studies with biopolymer-derived pharmaceutical materials, including microcrystalline cellulose obtained from lignocellulosic biomass, have demonstrated the importance of systematic material characterization in establishing their technological functionality and suitability for pharmaceutical applications.[15] Within this context, zein has emerged as a promising biopolymeric nanocarrier due to its biocompatibility, biodegradability, and ability to incorporate hydrophobic bioactive compounds and modulate their release.[16,17] However, zein nanoparticles have an inherent tendency toward aggregation, which can compromise their colloidal stability.[18,19] Various stabilization approaches involving surfactants,[20] proteins,[21] and polysaccharides[22] have therefore been investigated to improve the stability and functional properties of zein nanoparticles.[23]

Gum ghatti (GG), a natural gum obtained from the bark of *Anogeissus latifolia*, has attracted interest as a potential material for colon-oriented drug-delivery systems.[24] Traditionally used in food and Ayurvedic preparations, GG is increasingly being investigated due to its distinctive physicochemical and functional properties.[25] Chemically, GG is an acidic heteropolysaccharide composed predominantly of arabinose, galactose, mannose, and uronic acids, which contribute to its negative charge and aqueous dispersibility.[26] An important pharmaceutical characteristic of GG is its relative resistance to the acidic gastric environment and upper gastrointestinal digestion, while its polysaccharide structure can undergo degradation by colonic microbial enzymes.[24] These properties provide a rationale for investigating GG in formulations intended to modulate drug release along the gastrointestinal tract.

GG also exhibits useful emulsifying properties and stability over a range of pH and ionic conditions,[27,28] characteristics that may be advantageous for nanoparticle systems susceptible to aggregation under gastrointestinal conditions. Furthermore, its hydroxyl and carboxyl-containing groups provide opportunities for non-covalent association with protein-based carriers such as zein.[25] Thus, GG represents a promising natural material for stabilizing zein nanoparticles and modifying their interfacial and gastrointestinal release characteristics. Although GG has long been utilized as a food stabilizer and thickening agent, its application as a stabilizing and coating material for zein-based nanoparticle drug-delivery systems remains comparatively less explored.

In this context, the present study investigates GG as a natural stabilizing and coating material for RSV-loaded zein nanoparticles. The formulation strategy was designed to combine the hydrophobic drug-incorporating capability of zein with the stabilizing and gastrointestinal-responsive properties of GG. To the best of our knowledge, the

use of GG-associated zein nanoparticles for the delivery of RSV has not been previously reported. The developed system was therefore evaluated for its physicochemical characteristics, *in vitro* gastrointestinal release behavior, antioxidant activity, cytotoxicity against COLO-205 cells, and storage stability to establish its potential as an oral RSV delivery platform.

EXPERIMENTAL

Material

Gum ghatti was obtained from TCI Chemical (India) Pvt. Ltd., and trans-resveratrol ($C_{14}H_{12}O_3$) was purchased from Research-Lab Fine Chem Industries. The 2,2-diphenyl-1-picrylhydrazyl (DPPH) was purchased from HiMedia Laboratories, Thane, Maharashtra. Sodium hydroxide (NaOH), hydrochloric acid (HCl) and ethanol (purity about 99%) were provided by Loba Chemical, Mumbai, India.

Methods

Preparation of drug-loaded zein nanoparticles

The antisolvent precipitation method was employed to produce zein nanoparticles loaded with RSV (RZ-NP).[29] A stock solution of zein (400 mg, 30:70 v/v water/ethanol) was prepared. The resulting solution was then magnetically stirred (600 rpm) for 30 minutes. The zein stock solution was then supplemented with the addition of RSV (50 mg). The RSV zein stock solution was then diluted 1:4 with deionized water and added dropwise, in 5 mL increments, to the deionized water. The mix was then stirred for 2 h at room temperature. The ethanol in the RZ-NP dispersion was removed by using a rotary evaporator for 30 min at 40 °C. An equivalent volume of distilled water was added to make up for the loss of water. The pH of the mixture obtained was adjusted to 3.5.

Preparation of GG coated RZ-NP nanoparticles

Air drying the gum was performed, followed by grinding it with a high-speed mechanical blender into a fine powder. Various concentrations of GG were prepared as stock solutions (10 mg, 20 mg, 50 mg, 100 mg and 200 mg). To ensure the complete dissolution of the powder in deionized water, the mixture was magnetically stirred at room temperature. For preparation of complex particle dispersions, the pH of GG solutions was adjusted to 3.5, and a series of dropwise additions of RZ-NP nanoparticles were made to the GG solution. This mixture was then magnetically stirred for 30 min, at 600 rpm. The zein-to-GG ratios of the complex nanoparticle dispersions were 10:1, 5:1, 2:1, 1:1 and 1:2 (w/w), and are referred to herein as RZGG-$NP_{10:1}$, RZGG-$NP_{5:1}$, RZGG-$NP_{2:1}$, RZGG-$NP_{1:1}$, and RZGG-$NP_{1:2}$, respectively.

Physicochemical, spectral, morphological, and thermal characterization

The physicochemical characteristics of the prepared nanoparticles were evaluated in terms of mean particle size, polydispersity index (PDI), and ζ-potential using a Zetasizer Nano-ZS90 (Malvern Instruments, UK). Freshly prepared colloidal dispersions were appropriately diluted with deionized water prior to measurement and analyzed at 25 °C using a scattering angle of 90°. Measurements were performed using three independently prepared samples for each formulation (n = 3), and the results are expressed as mean ± standard deviation (SD).

Fourier-transform infrared (FTIR) spectroscopy was employed to characterize RSV, zein, GG, RZ-NPs, and RZGG-NPs and to examine changes in their characteristic functional-group absorption bands following nanoparticle formation. FTIR spectra were recorded using a Bruker Vertex 70/Alpha II spectrometer (Bruker, Germany) over the wavenumber range of 4000–400 cm^{-1} at room temperature (25 °C).

The morphology of the nanoparticles was examined by scanning electron microscopy (SEM). An aliquot of the nanoparticle dispersion was placed on an aluminium specimen holder and allowed to dry before analysis. The dried samples were mounted on conductive carbon tape and sputter-coated with a thin layer of gold/platinum to improve electrical conductivity. Representative SEM micrographs were subsequently acquired to evaluate particle morphology and surface characteristics.

Thermal characteristics of RSV, the individual carrier materials, and the nanoparticle formulations were evaluated by differential scanning calorimetry (DSC). Approximately 10 mg of each sample was placed in an aluminium pan and analyzed using a DSC instrument (Netzsch, Selb, Germany). Samples were heated to 350 °C at a heating rate of 10 °C/min under a nitrogen atmosphere maintained at a flow rate of 20 mL/min. The resulting thermograms were examined for changes in thermal transitions associated with nanoparticle formation and the physical state of RSV.

The solid-state characteristics of the samples were further investigated using wide-angle X-ray diffraction (XRD; Bruker D8, Germany). Diffraction patterns were recorded using Cu Kα radiation generated at an accelerating voltage of 40 kV and a current of 40 mA. Samples were scanned over a 2θ range of 5–50° using a step size of 0.02°. The diffraction profiles were used to assess changes in the detectable crystallinity of RSV following incorporation into the nanoparticle formulations.

Fluorescence measurements were performed using a spectrofluorometer (JASCO International Co., Ltd., Japan) at 25 °C. Prior to analysis, the nanoparticle dispersions were diluted with deionized water to a final nanoparticle concentration of 0.2 mg/mL, and the pH was adjusted to 3.5. The samples were excited at 280 nm, and emission spectra were recorded over the range of 290–450 nm.

Encapsulation efficiency (EE) and loading capacity (LC)

EE and LC of RSV in the RZGG-NPs were determined using a previously reported method with appropriate modifications.[30] Briefly, 1 mL of freshly prepared nanoparticle dispersion was mixed with 4 mL of ethanol to disrupt the nanoparticles and extract the encapsulated RSV. The mixture was centrifuged at 10,000 × g for 30 min, and the RSV content in the resulting supernatant was quantified spectrophotometrically at 307 nm using a UV-1800 spectrophotometer. RSV concentration was calculated from a calibration curve prepared under identical analytical conditions ($R^2 = 0.999$). Measurements were performed using three independently prepared samples ($n = 3$), and the results are expressed as mean ± standard deviation (SD).

Encapsulation efficiency and loading capacity were calculated using Equations (1) and (2), respectively:

$$EE(\%) = \frac{\text{Total RSV mass (mg)} - \text{free RSV mass (mg)}}{\text{Total RSV mass (mg)}} \times 100 \quad (1)$$

$$LC(\%) = \frac{\text{Total RSV mass (mg)} - \text{free RSV mass (mg)}}{\text{Total mass of nanoparticles}} \times 100 \quad (2)$$

In-vitro *release profile*

The *in vitro* release profiles of free RSV, RZ-NPs, and RZGG-$NP_{2:1}$ were evaluated using a dialysis membrane method under sequential simulated gastrointestinal conditions. Samples equivalent to 5 mg RSV were separately placed in prehydrated dialysis bags (MWCO 10 kDa). Simulated gastric fluid (SGF; pH 1.2) contained 2.0 g NaCl, 3.2 g pepsin, and 7.0 mL HCl per litre, whereas simulated intestinal fluid (SIF; pH 6.8) contained 6.8 g KH_2PO_4, 0.896 g NaOH, 10.0 g trypsin, and 3.0 g bile salts per litre. The dialysis bags were immersed in 150 mL SGF for the first 2 h and subsequently transferred to 150 mL SIF for an additional 10 h. The media were maintained at 37 ± 0.5 °C and 100 rpm. Samples (5 mL) were withdrawn at 30, 60, 90, 120, 150, 180, 210, 240, 300, 360, 420, 480, 540, 600, 660, and 720 min and immediately replaced with an equal volume of fresh, pre-equilibrated medium.

For RSV quantification, 1 mL of each collected sample was extracted with methanol, ultrasonicated for 10 min, and centrifuged at 8000 × g for 15 min. RSV in the supernatant was quantified spectrophotometrically at 307 nm. Experiments were performed in triplicate (n = 3), and results are expressed as mean ± SD. Cumulative RSV release was corrected for drug removed during successive sampling using:

$$Q_n = C_n V + V_s \sum_{i=1}^{n-1} C_i \quad (3)$$

where $C_n$is the RSV concentration at the n^{th}sampling point, $V$is the total medium volume (150 mL), $V_s$is the sampling volume (5 mL), and C_i represents concentrations in previously withdrawn samples. Percentage cumulative release was calculated relative to the initial RSV amount (5 mg).

Release data were further fitted to zero-order, first-order, Higuchi, Hixson–Crowell, and Korsmeyer–Peppas models, and goodness of fit was assessed from the coefficient of determination (R^2). The initial release region (≤60%) was used for Korsmeyer–Peppas analysis.[31]

Antioxidant activity

The antioxidant activity of the samples was measured according to a previously published method. Concentrations of RZGG-NPs and RSV, in ethanol, were prepared. The samples were added to a solution of 100 µM 1,1-diphenyl-2-picrylhydrazyl (DPPH) in ethanol in equal volumes, and left in the dark at room temperature for 30 min. A UV-visible spectrophotometer was used to determine absorbance of the reaction mixture at 517 nm. The antioxidant activities of L-Ascorbic acid and empty nanoparticles were compared as reference standards. The percentage of DPPH scavenging was calculated with the following Equation (4):

$$\text{DPPH scavenging percentage (\%)} = \left(\frac{AC - AS}{AC}\right) \times 100 \quad (4)$$

The absorbance of the control reaction was represented as AC, and the absorbance of the test sample was represented as AS.

Cell cytotoxicity

COLO-205 cells were seeded in 96-well microplates at a density of 1 × 10^4 cells/well in 100 µL of culture medium and allowed to adhere for 24 h at 37 °C in a humidified atmosphere containing 5% CO_2. The cells were subsequently treated with the test samples at concentrations of 20, 40, 60, 80, and 100 µg/mL, with each treatment performed in triplicate. Appropriate vehicle and untreated cell controls were included. Following treatment, the plates were incubated for an additional 24 h under the same conditions.

After the treatment, the culture medium was removed and 20 µL of MTT solution (5 mg/mL in PBS) was added to each well, followed by incubation for 4 h at 37 °C under 5% CO_2 to allow formation of formazan crystals by metabolically active cells. The MTT-containing medium was then carefully removed, and 200 µL of DMSO was added to each well to dissolve the resulting formazan crystals. The plates were protected from light and incubated for 10 min at 37 °C before subsequent measurement of formazan absorbance.

Storage stability studies

The short-term physical stability of RZ-NPs and optimized RZGG-$NP_{2:1}$ dispersion was evaluated over a period of 30 days. Freshly prepared nanoparticle dispersions were transferred to tightly closed containers, protected from light, and stored at 4 °C. Particle size, polydispersity index (PDI), and ζ-potential were determined at the beginning of the study and after 30 days of storage using the procedure described above. Measurements were performed using three independently prepared samples (n = 3), and the results

are expressed as mean ± standard deviation (SD). Changes in particle size, PDI, and ζ-potential were used to assess the short-term physical stability of the colloidal dispersions during storage.

Statistical analysis

Data are expressed as mean ± SD from three independent experiments or preparations ($n = 3$), unless otherwise stated. Technical measurements from the same sample were not considered independent replicates. Statistical analysis was performed using GraphPad Prism Version 9 (GraphPad Software, San Diego, CA, USA). Multiple-group comparisons were analyzed by one-way ANOVA followed by Tukey's post-hoc test. For concentration-dependent cytotoxicity data, two-way ANOVA followed by Šídák's multiple-comparison test was used. Statistical significance was set at $p < 0.05$. IC_{50} values were estimated by nonlinear regression of concentration–response data using a four-parameter logistic model and reported with 95% confidence intervals.

RESULTS AND DISCUSSION

Determination of particle size and zeta-potential

Mean particle size, PDI, zeta potential are important parameters for the assessment of nanoparticle stability and uniformity. The results (Table 1) obtained from the characterization of the nanoparticles (RZ-NPs or RZGG-NPs) loaded with RSV at different GG concentration levels provide an insight into the effect of GG on the physicochemical characteristics of the nanoparticles. The RZ-NP without GG had an average particle size of 107.9 nm, which is associated with good particle dispersion of antisolvent precipitated zein nanoparticles. The relatively small size indicates efficient formation of nanoparticles under the mentioned conditions.[32,33]

The results clearly reveal that the quantity of GG used in the formulation of nanoparticles significantly influences the size and uniformity of the nanoparticles. Such characteristics are relevant, as they can influence over time the stability of the nanoparticles and their potential body-to-body consistency of reactivity. At a low GG concentration (zein:GG ratio of 10:1), the particles were quite large (222.3 nm), and the PDI was high (0.482), indicating that the particles varied widely in size. The above indicates that the use of a small quantity of GG did not provide enough coverage of the surface of zein particles. If not covered properly, the particles will tend to stick or aggregate, which is why the increase in size is noticeable, and uniformity is not good. Additionally, a study on fucoidan-coated zein nanoparticles that examined the effect of high zein-to-fucoidan ratio (40:1) on fucoidan content and particle aggregation indicated that high ratios of 40:1 led to significant particle aggregation, as the electrostatic repulsion and surface coating by fucoidan were inadequate. This led to large-sized particles, which were not stable and to the presence of noticeable particles or precipitates, emphasizing the need for a high concentration of polymer as was seen in this study with low levels of GG.[34]

When the GG concentration was increased slightly (5:1 ratio), there was some improvement. The particle size was slightly smaller (212.5 nm) and the PDI was a little smaller (0.326), however PDI was still relatively large, meaning there was a large spread of particle sizes. This means that the nanoparticles were not completely stabilized by the added GG, but it reduced some aggregation.

A critical ratio of zein-to-GG was found at 2:1. In this case, the nanoparticles were found to be smaller (165.4 nm) and much more uniform (low PDI 0.164). This means that was the proper amount of GG, enough to coat each particle, so that it did not adhere to other particles. This is known as "steric stabilization" and is achieved by providing a protective barrier around the particles to prevent them from coming into close contact and clumping together.[35] The study on fucoidan coated zein nanoparticles was particularly useful because the researchers found that the best particle size reduction and PDI (less than 0.2) occurred at the ratio of 2:1 zein: fucoidan, which further validates this observation. Similar to GG, fucoidan was able to provide an effective surface coating and the quantity needed to prevent aggregation or over-coating was fine-tuned.[36]

Interestingly, when even more GG was used (ratios of 1:1 and 1:2), the particle size was marginally increased (174.0 nm and 182.6 nm), but the PDI remained unchanged (0.160 and 0.191), indicating that even then the particle size was not significantly distributed. The minor growth in size may be attributed to the growth of a thicker GG layer around each particle. This layer does not lead to aggregation, but rather to somewhat bulkier particles. Others have reported that an increase in the concentration of a polymer also slightly increases the size of the nanoparticles and promotes stability and uniformity.[36]

The zeta potential is one of the most important parameters that indicate the surface charge of the nanoparticles and the colloidal stability of

nanoparticles. The zeta potential of RZ-NP was determined as +23.24 mV, which is the result of the zein's cationic character at acidic pH of the nanoparticles formulation. The electrostatic repulsion due to this positive surface charge helps to stabilize the nanoparticles, ensuring that they do not aggregate. After the addition of GG, which is an anionic polysaccharide, the zeta potential reached negative values, confirming that GG molecules were able to coat the zein nanoparticles. When zein content to GG ratio is 10:1, the zeta potential is reduced to -11.08 mV. This partial negative shift indicated that the GG was not covering the surface completely, which was not enough for the full stabilization of the nanoparticles, resulting in aggregation, as seen from the large particle size and high PDI.[36]

The zeta potential became more negative at -19.15 mV as the GG concentration increased to 5:1, which indicates that the surface coverage was getting better, but not complete. The relatively high particle size and PDI indicated that the nanoparticles had a tendency to aggregate.

The zeta potential further dropped to -24.58 mV at the 2:1 ratio, showing complete coverage of the surface with GG, which results in optimal stabilization. This gives rise to high electrostatic repulsion between the particles, thus the particles do not aggregate, and smaller and uniform nanoparticles are obtained. In higher GG concentrations (1:1 and 1:2), the zeta potential remained strongly negative (-23.40 mV to -21.90 mV), thus maintaining the colloidal stability of the system both electrostatic and steric.

The results of this study show that the concentration of GG is a key factor to control the size, uniformity and stability of zein-based nanoparticles. The best zein-to-GG ratio was 2:1, which resulted in the production of nanoparticles with a narrow size distribution and good stability. Electrostatic and steric interactions are the major interactions between zein nanoparticles and GG.

Table 1
Various combinations of zein-to-GG ratios and associated properties of the resultant complex particles, their encapsulation efficiency and loading capacity

Samples	Zein conc. (mg/mL)	Gum ghatti conc. (mg/mL)	Mean particle size (nm)	Polydispersity index (PDI)	ζ-potential (mV)	Physical stability	Entrapment efficiency (%)	Loading capacity (%)
RZ-NP	5	-	107.9 ± 4.02	0.241 ± 0.001	+23.24 ± 2.23	Stable	56.48 ± 0.01 %	4.35 ± 0.01%
RZGG-$NP_{10:1}$	5	0.5	222.3 ± 7.33	0.482 ± 0.003	-11.08 ± 1.88	Aggregated	68.72 ± 0.23 %	5.62 ± 0.05%
RZGG-$NP_{5:1}$	5	1	212.5 ± 9.72	0.326 ± 0.004	-19.15 ± 3.65	Aggregated	76.88 ± 0.02 %	9.73 ± 0.04%
RZGG-$NP_{2:1}$	5	2.5	165.4 ± 3.62	0.164 ± 0.001	-24.58 ± 1.09	Stable	84.64 ± 0.01 %	14.19 ± 0.01 %
RZGG-$NP_{1:1}$	5	5	174 ± 5.92	0.160 ± 0.002	-23.40 ± 3.30	Stable	80.08 ± 0.02 %	12.39 ± 0.03 %
RZGG-$NP_{1:2}$	5	10	182.6 ± 7.40	0.191 ± 0.003	-21.90 ± 2.48	Stable	76.32 ± 0.03 %	10.24 ± 0.02 %

Values are expressed as mean ± SD (n = 3 independent experiments). Particle size and ζ-potential are reported in nm and mV, respectively; PDI is dimensionless

Encapsulation efficiency (EE) and loading capacity (LC)

The efficacy of the engineered delivery system that encapsulates RSV was assessed by capturing the EE and LC of the nanoparticles (Table 1). These parameters can offer insight into the degree of encapsulation of RSV into the nanoparticles and into the amount of RSV loaded and the mass of the nanoparticles.

The EE of the zein-containing nanoparticles (RZ-NP) showed a relatively low value of 56.48 ± 0.014%. This indicated that there is a large fraction of RSV present in the nanoparticles that was not effectively encapsulated, possibly because of the poor encapsulation efficiency of zein alone. When GG was added to the formulation, there was a significant improvement in EE. At a 2:1 zein-to-GG ratio, EE increased significantly ($p<0.05$) to 84.64 ± 0.017%. The improvement can be attributed to the effective stabilization that GG provides, not only in preventing nanoparticle aggregation, but also in providing extra binding

sites and a more stable core-shell structure for the RSV to be encapsulated within.

As GG concentrations increased further, EE showed a slight decline, with values of 80.08 ± 0.024% at a 1:1 ratio and 76.32 ± 0.033% at a 1:2 ratio. The decrease may be attributed to the high concentration of GG that could result in less zein matrix available to properly encapsulate RSV, or it could be the result of a higher concentration of GG disrupting the interactions between zein and RSV.

The LC of RSV followed a trend similar to that of the EE. The LC for the RZ-NP was relatively low, at 4.35 ± 0.01%, which meant that only a small fraction of RSV was incorporated into the nanoparticles, compared to the total mass of the RSV. The increase of GG significantly enhanced the LC with the best result being obtained from 2:1 zein-to-GG ratio (14.19 ± 0.01%). At the concentration used, the optimal ratio was produced where the balance between zein and GG enabled the incorporation of the highest amount of RSV.

As the GG concentration increased to 1:1 and 1:2 ratios, the LC decreased slightly to 12.39 ± 0.03% and 10.24 ± 0.02%, respectively. The dilution effect may be responsible for this decrease in LC at higher GG concentrations as the mass of GG particles increased in the presence of a fixed amount of RSV, resulting in a lower percentage of RSV in the total mass of the nanoparticles.

The results showed that the encapsulation efficiency and loading capacity of RSV were drastically improved when GG was added to the zein nanoparticle formulation, especially in the formulation with zein-to-GG ratio of 2:1. This balance was crucial to ensure that the nanoparticles were adequately stabilized by GG, enabling efficient RSV encapsulation without over-diluting or interfering with the formulation.

Fluorescence spectroscopy

When used to study the fluorescence behaviour of fluorophores in various surroundings, fluorescence spectroscopy is a useful tool for exploring intermolecular interactions.[30] Upon excitation at 280 nm, zein exhibits a fluorescence emission peak at 304 nm and is composed mainly of tyrosine residues that are responsible for this fluorescence (Fig. 1).[37] When RSV was encapsulated, however, the fluorescence of tyrosine was greatly quenched, and the λ_{max} was greatly red shifted. This shift is a result of the polarity of the local environment around the fluorophore increasing. The quenching of zein fluorescence was more significant than the other proteins, and the appearance of a new fluorescence peak at about 380 nm, which corresponds to maximum emission of RSV. The addition of GG to the system further decreased the fluorescence intensity of RSV. The decrease indicates that the local environmental polarity around the complexation of GG and zein and RSV is enhanced in the nanoparticles. The presence of a large number of tyrosine residues in zein gives rise to a characteristic peak of fluorescence emission at ~304 nm. Therefore, zein's intrinsic fluorescence spectrum is similar to tyrosine's. The fluorescence intensity of zein was significantly decreased when it interacted with GG, suggesting that the GG could quench the intrinsic fluorescence of zein. The electrostatic interaction between positively charged tyrosine (IEP = 5.66) and negatively charged GG could be responsible for this effect.[36]

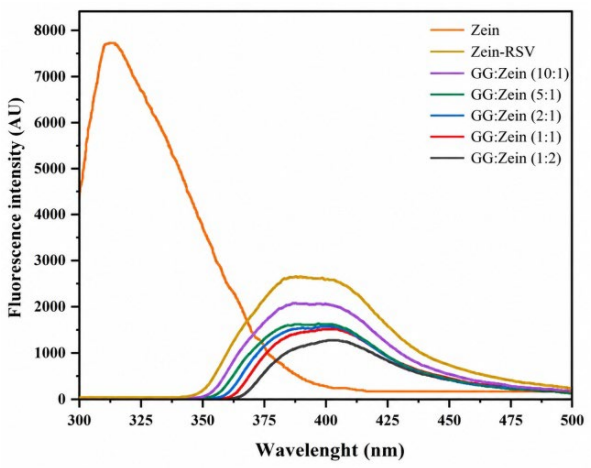


Figure 1: Fluorescence emission spectra of different concentrations of RZNGG-NP

The encapsulation process is carried out with the use of a polysaccharide and RSV and the non-covalent intermolecular interactions are responsible for the observed decrease in the fluorescence intensity. The result is in line with earlier work, which showed that protein fluorescence can be suppressed in the presence of anionic polysaccharides, like pectin.[38] The progressive decrease of the fluorescence intensity of the zein-GG complexes is further evidence that the higher the charge density of GG, the more quenching is enhanced. This is consistent with previous reports of a correlation between the charge density of polysaccharides and the fluorescence characteristics of protein-polysaccharide complexes.[36]

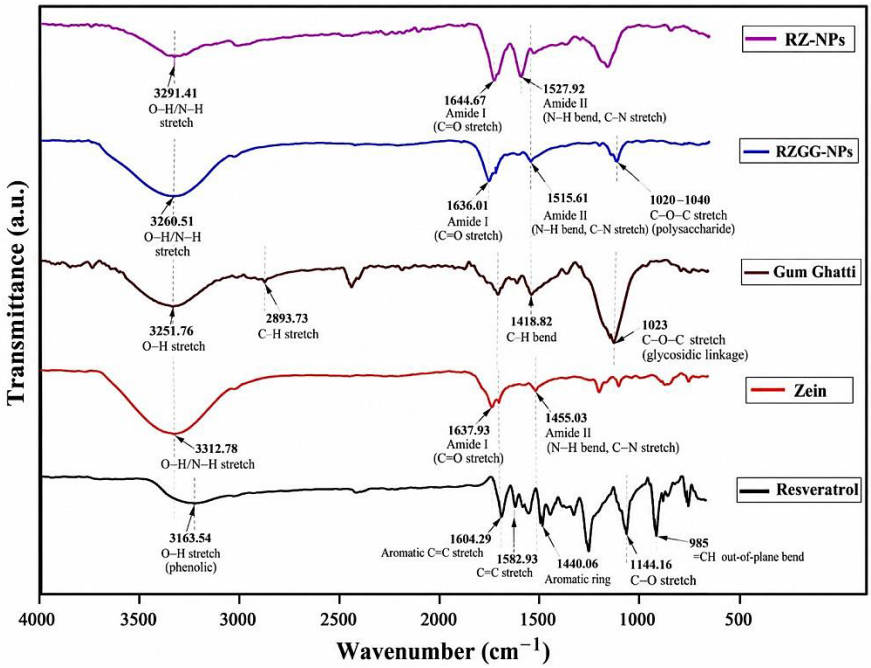


Figure 2: FTIR spectra of individual components and nanoparticle formulations

ATR-FTIR spectroscopy

The FTIR spectra of RSV, zein, gum ghatti (GG), RZ-NPs, and RZGG-NPs are presented in Figure 2. Zein exhibited a broad absorption band at 3312.78 cm^{-1}, attributable to O–H/N–H stretching, together with characteristic protein-associated bands at 1637.93 and 1455.03 cm^{-1}. These bands arise predominantly from vibrations associated with the peptide backbone and are characteristic of the protein structure of zein.[39]

Free RSV showed its characteristic spectral features, including a broad phenolic O–H stretching band at 3163.54 cm^{-1} and prominent bands at 1604.29 and 1582.93 cm^{-1} associated with its conjugated aromatic/olefinic structure. Additional bands at 1440.06, 1144.16, and 985 cm^{-1} were attributable to aromatic-ring, C–O, and trans-olefinic vibrations, respectively, confirming the characteristic polyphenolic structure of RSV. GG exhibited a broad O–H stretching band at 3251.76 cm^{-1}, C–H stretching at 2893.73 cm^{-1}, and characteristic bands at 1418.82 and 1023 cm^{-1}, the latter being associated with C–O/C–O–C vibrations of its polysaccharide backbone and glycosidic linkages.[40]

Distinct spectral changes were observed following nanoparticle formation. In RZ-NPs, bands were observed at approximately 3291.41, 1644.67, and 1527.92 cm^{-1}, while RZGG-NPs showed a broad O–H/N–H band around 3260.51 cm^{-1} together with bands at approximately 1636.01 and 1515.61 cm^{-1}. The shifts and broadening observed particularly in the O–H/N–H and amide regions demonstrate modification of the local chemical environment of zein following incorporation of RSV and association with GG. These spectral changes are consistent with the establishment of non-covalent intermolecular associations, potentially involving hydrogen bonding and other interactions between the protein, polysaccharide, and RSV.[41]

Several characteristic RSV bands became markedly attenuated or were no longer individually resolved in the spectra of the nanoparticle formulations. This observation is consistent with incorporation of RSV within the zein-based matrix,

where its spectral contribution may be reduced by molecular dispersion, its relatively low proportion in the formulation, and overlapping absorption bands of the carrier components. Importantly, the RZGG-NP spectrum retained the characteristic polysaccharide-associated C–O/C–O–C absorption region, together with alterations in the zein amide bands, providing supportive evidence for the association of GG with the RSV-loaded zein nanoparticle system.

Overall, the preservation of characteristic functional-group regions together with systematic shifts, broadening, and attenuation of selected bands provides complementary evidence for the successful formation of the RSV-loaded zein–GG nanoparticle system and modification of the molecular environment of its constituent components. The absence of prominent new absorption bands further suggests that nanoparticle formation occurred predominantly through non-covalent associations rather than formation of new covalent functionalities. These observations are consistent with previously reported protein–polysaccharide complexation behavior.[41] While FTIR cannot independently establish the precise nature or strength of individual molecular interactions, the spectral findings provide strong supportive physicochemical evidence for the intended nanoparticle composition and organization.

X-ray diffraction (XRD)

The XRD patterns of RSV, zein, GG, RZ-NPs, and RZGG-NPs are presented in Figure 3 and provide insight into changes in the crystalline characteristics of RSV following nanoparticle formation. Pure RSV exhibited several sharp and well-defined diffraction peaks at 2θ = 6.76°, 13.38°, 16.51°, 19.37°, 22.51°, 23.77°, 25.39°, and 28.47°, confirming its highly crystalline nature. In contrast, zein displayed broad diffraction features around 8.8° and 19.3°, consistent with its partially ordered protein structure, while GG showed a broad diffuse halo centered at approximately 20°, characteristic of its predominantly amorphous polysaccharide structure.

A marked alteration in the diffraction pattern was observed following incorporation of RSV into zein nanoparticles. In RZ-NPs, the sharp characteristic reflections of crystalline RSV were substantially attenuated or no longer detectable, while the broad diffraction features associated with the zein matrix predominated. This finding indicates a pronounced reduction in the detectable crystalline order of RSV following encapsulation and is consistent with its dispersion within the zein nanoparticle matrix in a less ordered or predominantly amorphous state.[42]

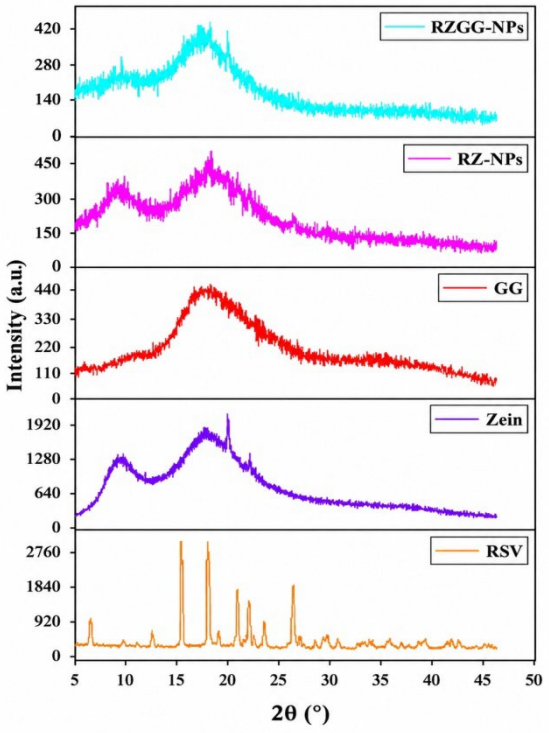


Figure 3: XRD patterns of individual components and nanoparticle formulations

The RZGG-NPs similarly lacked the distinct sharp diffraction peaks characteristic of free RSV and exhibited a predominantly broad diffraction profile reflecting contributions from the zein and GG matrices. The persistence of a broad feature around the region characteristic of GG is consistent with the presence of the polysaccharide in the formulated nanoparticles. Importantly, the absence of prominent RSV crystalline reflections after GG association indicates that RSV remained in a state of markedly reduced detectable crystallinity within the final RZGG-NP formulation.

Overall, the XRD results provide strong supportive evidence that nanoparticle formation substantially altered the solid-state organization of RSV, with the drug no longer exhibiting the pronounced crystalline diffraction pattern observed in its free form. Together with the characteristic broad features of zein and GG, these findings support the successful incorporation of RSV within the zein–GG nanoparticle system. However, the attenuation or disappearance of RSV diffraction peaks is interpreted as evidence of reduced detectable crystallinity rather than definitive proof of complete amorphization, since factors such as drug loading, dilution within the carrier matrix, and detection sensitivity may also influence the observed diffraction pattern.

Differential scanning calorimetry (DSC)

The thermal behavior and physical state of RSV, zein, GG, RZ-NPs, and RZGG-NPs were evaluated by DSC, and the thermograms are presented in Figure 4. Pure RSV (Fig. 4a) exhibited a distinct and sharp endothermic peak at 267.38 °C, characteristic of its crystalline melting transition and confirming the highly ordered crystalline nature of the free drug. Zein (Fig. 4b) displayed a broad endothermic transition at approximately 88.10 °C, primarily associated with the release of absorbed and bound water from the protein matrix.[43] Similarly, GG (Fig. 4c) showed a broad endothermic event at approximately 106.12 °C, consistent with moisture loss from its hydrophilic polysaccharide structure.

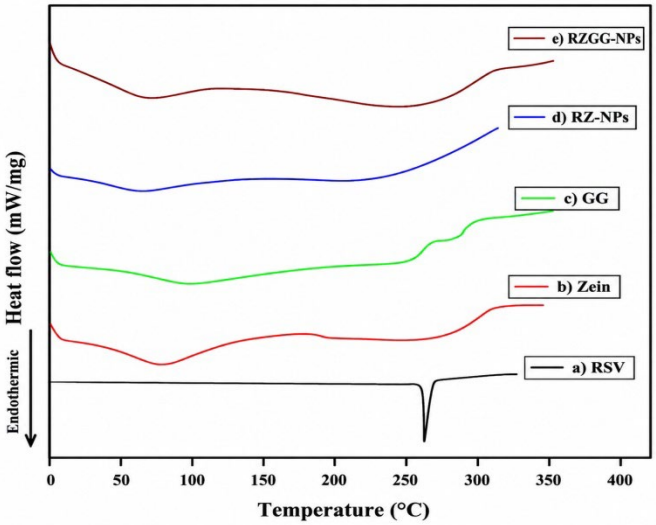


Figure 4: DSC thermograms of individual components and nanoparticle formulations: (a) RSV, (b) zein, (c) gum ghatti (GG), (d) RZ-NPs, and (e) RZGG-NPs

Notably, nanoparticle formation produced a pronounced alteration in the thermal behavior of RSV. In both RZ-NPs (Fig. 4d) and RZGG-NPs (Fig. 4e), the characteristic sharp melting endotherm of crystalline RSV at 267.38 °C was no longer distinctly detectable. This marked change indicates a substantial reduction in the detectable crystalline character of RSV following its incorporation into the zein-based nanoparticles and is consistent with its dispersion within the carrier matrix in a less ordered or predominantly amorphous state. The thermal behavior of the final formulation was instead dominated by the broader transitions associated with the carrier matrix, supporting effective incorporation of RSV into the nanoparticulate system.

The DSC findings were further supported by the XRD results, in which the characteristic sharp diffraction peaks of crystalline RSV were markedly attenuated or no longer detectable in RZ-

NPs and RZGG-NPs. Thus, the complementary DSC and XRD findings consistently demonstrate a pronounced alteration in the solid-state organization of RSV following nanoparticle formation. Importantly, the reduced crystalline character was maintained after association with GG, indicating that formation of the final RZGG-NP system did not restore the original crystalline state of RSV.

Overall, the complementary DSC and XRD findings provide strong physicochemical evidence for the successful incorporation of RSV within the zein–GG nanoparticle matrix and a pronounced reduction in its crystalline order following nanoparticle formation. The disappearance of the characteristic RSV melting endotherm, together with the marked attenuation of its crystalline diffraction peaks, suggests that RSV was effectively dispersed within the carrier matrix in a less ordered state. This alteration in solid-state characteristics is particularly relevant for a poorly water-soluble compound such as RSV, as reduction in crystalline order can decrease the crystal-lattice energy barrier associated with dissolution. Moreover, the maintenance of this modified solid-state profile in RZGG-NPs indicates that subsequent association with GG preserved the physicochemical state achieved during nanoparticle formation. Thus, the DSC findings, in conjunction with XRD analysis, support effective incorporation and solid-state modification of RSV within the developed zein–GG nanoparticle system.

Scanning electron microscopy (SEM)

SEM was used to analyze the morphological characteristics of zein nanoparticles (ZN-NPs), RZ-NP and RZNGG-NPs. The SEM image (Fig. 5A) showed the surface of zein NPs to be smooth and spherical, indicating their well-defined structure. On the other hand, when RSV was encapsulated inside the zein NPs, the RZ-NPs were densified and irregularly shaped spherical NPs, as seen in Figure 5B. Further observations showed that these nanoparticles had an irregular rough surface, which was probably caused by a small fraction of RSV remaining on the surface. The shape of these nanoparticles is sticky, flaky and compact, possibly due to the hydrophobic interactions among different components, which lead to aggregation and the resulting necklace like structure. Based on these observations, it can be concluded that most of the RSV was successfully encapsulated inside the zein NPs, but some RSV could be attached to the surface.

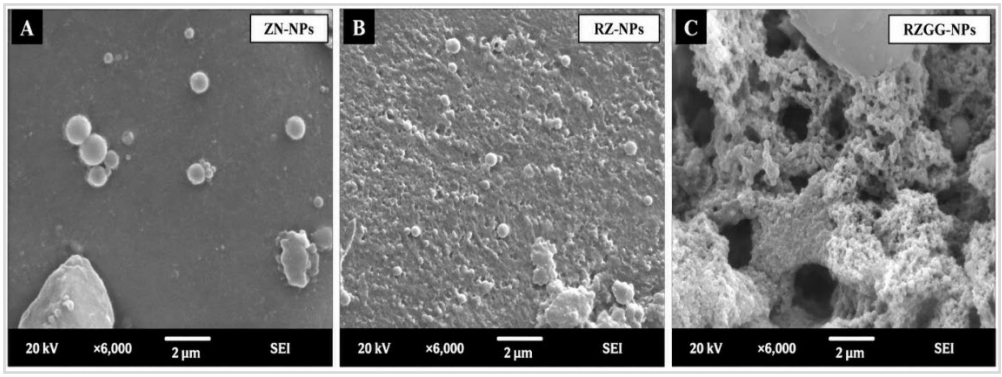


Figure 5: SEM images showing the surface morphology of (A) ZN-NPs, (B) RZ-NPs, and (C) RZGG-NPs (micrographs recorded at ×6,000 magnification and 20 kV accelerating voltage)

To overcome the above problem, GG was introduced. Interestingly, the surface and morphology of zein NPs was changed upon addition of GG, leading to a close-packed composite in the case of RZNGGs (Fig. 5C). This means that GG is very surface active and able to cover RSV that didn't get into the zein NPs. The particle size of the RZNGG-NPs however, was significantly larger than that of the zein NPs. This size increase can be attributed to the electrostatic interactions between the GG molecules and the surface of the zein NPs. Most importantly, the introduction of GG also reduced aggregation of the particles. The electrostatic forces between GG molecules and zein NPs were the stabilizing forces which prevented the aggregation of zein into larger aggregates. The surface of GG stabilized zein nanoparticles was more dispersible and stable due to this stabilization.

***In-vitro* release profile**

The *in vitro* release profiles of free RSV, RZ-NPs, and RZGG-NPs under sequential simulated gastrointestinal conditions are presented in Figure 6. During the initial gastric phase (SGF, pH 1.2; 0–120 min), the three samples exhibited distinctly different release profiles. At 120 min, approximately 6%, 38%, and 30% RSV release was observed from free RSV, RZ-NPs, and RZGG-NPs, respectively. The comparatively low apparent release of free RSV may be associated with its poor aqueous solubility, whereas incorporation into the zein-based nanoparticles increased the fraction of RSV available in the external release medium.

Following transfer to SIF (pH 6.8), RSV release from both nanoparticle formulations increased progressively. RZ-NPs showed the most rapid release, reaching approximately 98% at 720 min, whereas RZGG-NPs exhibited a comparatively slower and more prolonged release profile, reaching approximately 82% at 720 min. In contrast, free RSV showed substantially lower release, reaching approximately 42% at the end of the experiment. The slower release from RZGG-NPs relative to uncoated RZ-NPs is consistent with an additional diffusional barrier provided by the GG-rich interfacial layer. Hydration of the polysaccharide layer and diffusion of RSV through the hydrated zein–GG matrix may therefore have contributed to modulation of drug release. The results demonstrate that GG association altered the release behavior of RSV-loaded zein nanoparticles under the investigated gastrointestinal conditions.[44]

To further characterize the release behavior, the data were fitted to zero-order, first-order, Higuchi, Hixson–Crowell, and Korsmeyer–Peppas kinetic models (Table 2). Among the conventional models evaluated, both nanoparticle formulations showed the highest coefficient of determination for the Higuchi model, with R^2 values of approximately 0.995 for RZ-NPs and 0.996 for RZGG-NPs. RZGG-NPs also showed good agreement with the first-order (R^2 = 0.988) and Hixson–Crowell (R^2 = 0.989) models. The comparatively high Higuchi fit indicates that diffusion through the hydrated carrier matrix makes an important contribution to RSV release, although the close fits obtained with other models indicate that the release process should not be attributed to a single mechanism solely on the basis of R^2.

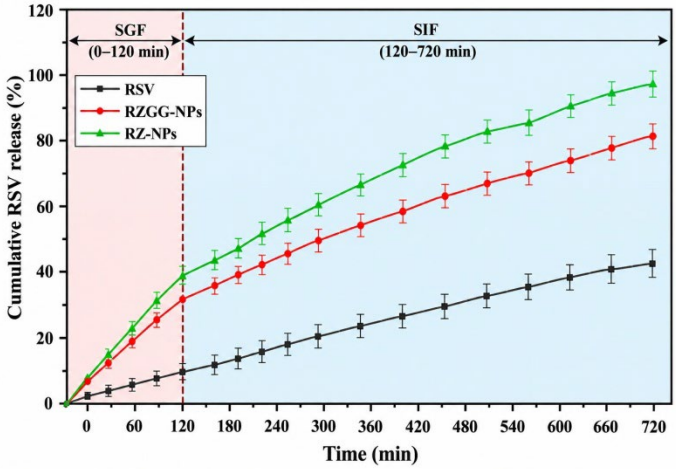


Figure 6: *In vitro* release profiles of free resveratrol RSV, RZ-NPs, and RZGG-NPs under sequential simulated gastrointestinal conditions (data presented as mean ± SD (n = 3))

Table 2
Kinetic modelling of *in vitro* RSV release profiles from RZ-NPs and RZGG-NPs using different mathematical release models

Formulation	Zero-order R^2	First-order R^2	Higuchi R^2	Hixson–Crowell R^2	Korsmeyer–Peppas R^2	Release exponent (n)	Suggested release behavior
RZ-NPs	0.948	0.891	0.995	0.982	0.978	0.883	Anomalous/non-Fickian
RZGG-NPs	0.955	0.988	0.996	0.989	0.973	0.796	Anomalous/non-Fickian

For the Korsmeyer–Peppas analysis, the initial portion of the release profile corresponding to ≤60% cumulative release was considered. The release exponent (n) was approximately 0.883 for RZ-NPs and 0.796 for RZGG-NPs. For approximately spherical particulate systems, these values are consistent with anomalous/non-Fickian transport, suggesting that RSV release may involve a combination of diffusion and relaxation or structural reorganization of the hydrated polymeric matrix rather than simple Fickian diffusion alone. In RZGG-NPs, the hydration of the GG-associated interfacial layer may additionally increase the diffusional path length and restrict rapid RSV diffusion, consistent with the slower release observed relative to RZ-NPs.[45]

Antioxidant activity (DPPH radical scavenging assay)

RSV possesses well-established antioxidant activity, which contributes to its potential health-promoting effects.[46] The incorporation of antioxidant compounds into nanoparticulate carriers may provide a useful approach for preserving their functional activity and potentially facilitating their delivery to biological sites of interest.[47] Accordingly, the DPPH radical-scavenging activities of unloaded zein–GG nanoparticles (ZGG-NPs), free RSV, and RSV-loaded zein–GG nanoparticles (RZGG-NPs) were evaluated over a concentration range of 10–50 µg/mL, with ascorbic acid (AA) used as the reference antioxidant (Fig. 7).

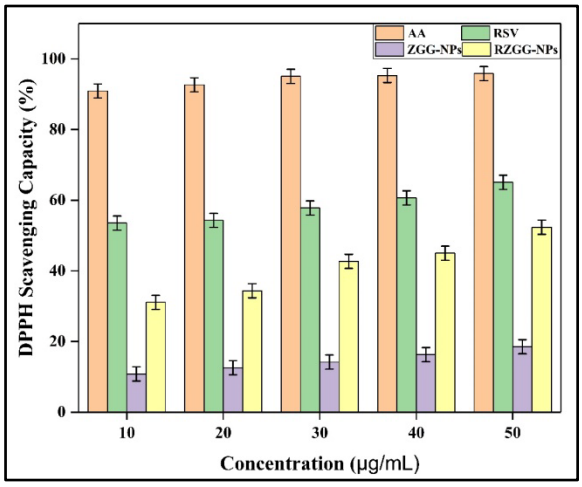


Figure 7: DPPH radical scavenging activity of (a) ascorbic acid, (b) blank zein–gum ghatti nanoparticles (ZGG-NPs), (c) RSV, and (d) RZGG-NPs at different concentrations. Data are presented as mean ± SD (n = 3)

All tested samples exhibited concentration-dependent radical-scavenging activity, with AA showing the highest response and reaching 95.80 ± 0.02% at 50 µg/mL. Free RSV also demonstrated substantial antioxidant activity, consistent with its reported ability to scavenge free radicals through hydrogen-atom transfer mechanisms.[48] At 10 µg/mL, the DPPH scavenging activities of free RSV, RZGG-NPs, and unloaded ZGG-NPs were 53.50 ± 0.06%, 31.10 ± 0.06%, and 10.84 ± 0.05%, respectively. The comparatively low activity of unloaded ZGG-NPs, which increased from 10.84 ± 0.05% to 18.54 ± 0.04% over the investigated concentration range, indicates that RSV was primarily responsible for the radical-scavenging activity of the drug-loaded formulation. This observation is also consistent with the comparatively lower antioxidant contribution of the carrier components.[49]

At 50 µg/mL, free RSV exhibited 65.04 ± 0.02% DPPH radical-scavenging activity compared with 52.37 ± 0.03% for RZGG-NPs. Thus, the present findings do not indicate enhancement of the intrinsic antioxidant activity of RSV following encapsulation. Rather, the substantial scavenging activity retained by RZGG-NPs demonstrates that RSV preserved its antioxidant functionality after incorporation into the zein–GG nanoparticle system. The lower apparent activity of RZGG-NPs relative to free RSV may be associated with reduced immediate accessibility of encapsulated RSV to DPPH radicals, as a proportion of RSV may remain entrapped within or associated with the nanoparticle matrix during the assay. Overall, the

results support retention of RSV antioxidant activity following nanoencapsulation rather than enhancement of its radical-scavenging capacity.

Cell cytotoxicity

The cytotoxic effects of free RSV and RZGG-NPs against COLO-205 cells were evaluated using the MTT assay, and the results are presented in Figure 8. Both free RSV and RZGG-NPs produced a clear concentration-dependent reduction in cell viability over the tested concentration range of 20–100 µg/mL. Free RSV reduced cell viability from approximately 80% at 20 µg/mL to 40% at 100 µg/mL, confirming the concentration-dependent cytotoxic potential of RSV against COLO-205 cells. Notably, RZGG-NPs produced a greater reduction in cell viability at corresponding RSV concentrations, decreasing viability from approximately 68% at 20 µg/mL to 35% at 100 µg/mL. Statistically significant differences between free RSV and RZGG-NPs were observed at the concentrations indicated in Figure 8. The reference drug 5-fluorouracil (5-FU) showed a pronounced concentration-dependent response, with cell viability decreasing from approximately 77% to 21% over the investigated concentration range.

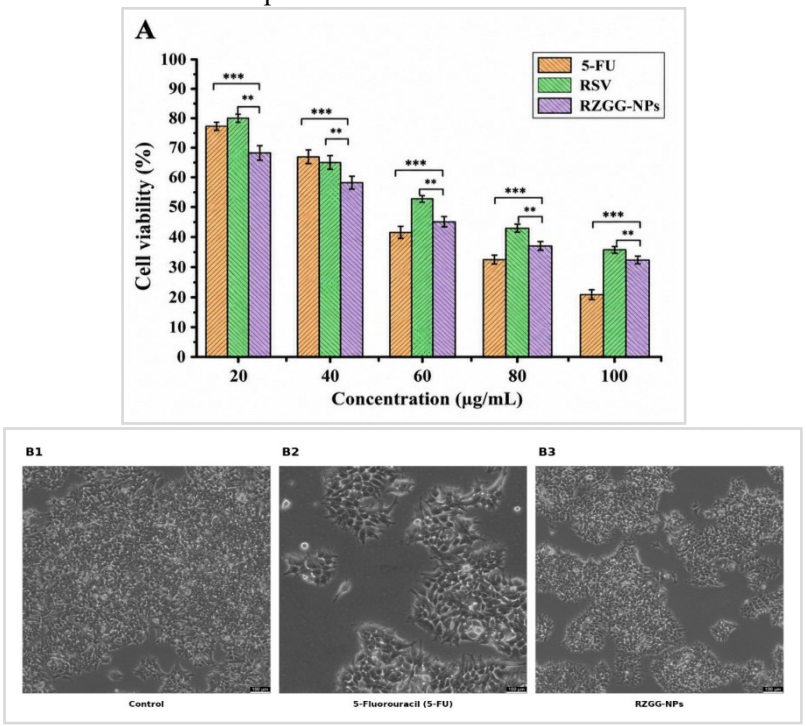


Figure 8: Cytotoxicity of RSV and RZGG-NPs against COLO-205 cells. (A) Cell viability of COLO-205 cells following treatment with 5-fluorouracil (5-FU), free RSV, and RZGG-NPs at concentrations of 20–100 µg/mL, as determined by the MTT assay (data presented as mean ± SD (n = 3); **p < 0.01 and ***p < 0.001); (B) Representative microscopic images of COLO-205 cells showing untreated control (B1), 5-FU-treated cells (B2), and RZGG-NP-treated cells (B3). Scale bar = 100 µm

Table 3
Particle size distribution and zeta potential of RZ-NPs and RZGG-NPs on days 1 and 30

Sample name	Days	Mean particle size (nm)	Polydispersity index	ζ-potential (mV)
RZ-NP	1	107.9 ± 3.24	0.241 ± 0.01	+23.24 ± 1.33
RZ-NP	30	413 ± 5.54	0.413 ± 0.02	+38.79 ± 2.12
RZGG-$NP_{2:1}$	1	165.4 ± 2.64	0.164 ± 0.02	-24.58 ± 2.19
RZGG-$NP_{2:1}$	30	178.6 ± 1.79	0.175 ± 0.02	-20.39 ± 1.79

Values expressed as mean ± SD (n = 3 independent experiments); Particle size and ζ-potential reported in nm and mV, respectively; PDI is dimensionless

The IC_{50} of RZGG-NPs was 57.28 µg/mL, as determined from the concentration–response data by nonlinear regression using a four-parameter logistic model. The consistently lower cell viability observed with RZGG-NPs, compared with free RSV, indicates that the incorporation of RSV into the zein–GG nanoparticle system favorably influenced its *in vitro* cytotoxic response in COLO-205 cells. The representative microscopic images (Fig. 8B) further supported the MTT findings, showing noticeable treatment-associated alterations in cell density and morphology compared with the untreated control.

The greater cytotoxic response of RZGG-NPs may potentially be associated with the nanoparticulate presentation of RSV and its interaction with the cellular environment. Nanoparticle–cell interactions, cellular internalization, and subsequent availability of RSV following its release from the carrier may contribute to the observed effect. However, these mechanisms were not directly investigated in the present study and therefore require confirmation through dedicated cellular uptake and intracellular drug-distribution studies. Importantly, the present findings demonstrate the effect under *in vitro* conditions and do not establish enhanced tumour penetration or *in vivo* bioavailability.

The observed findings are consistent with previous reports demonstrating favorable cellular responses following nanoencapsulation of RSV. RSV-loaded solid lipid nanoparticles and nanostructured lipid carriers have been reported to exhibit increased cytotoxic effects in Caco-2 cells.[50] Similarly, RSV-loaded zein/pectin nanoparticles showed greater inhibition of Bel-7402 cell proliferation than free RSV, with the response being dependent on RSV concentration. Although differences in nanoparticle composition and cell models should be considered, these reports support the potential of nanoparticulate systems to modulate the cellular response to RSV.

Overall, the results demonstrate that RZGG-NPs retained the cytotoxic activity of RSV and produced a greater concentration-dependent reduction in COLO-205 cell viability than free RSV under the investigated conditions. These findings provide encouraging *in vitro* evidence supporting further investigation of the zein–GG nanoparticle system as a carrier for RSV, particularly through mechanistic cellular studies and subsequent *in vivo* evaluation.

Storage stability studies

The short-term physical stability of RZ-NPs and RZGG-NP was evaluated by monitoring changes in particle size, PDI, and ζ-potential during storage at 4 °C for 30 days (Table 3). The two formulations exhibited distinctly different changes during the storage period. The mean particle size of uncoated RZ-NPs increased markedly from 107.9 to 413.0 nm, accompanied by an increase in PDI from 0.241 to 0.413. The simultaneous increase in hydrodynamic diameter and PDI indicates the development of larger particle populations, together with substantial broadening of the particle-size distribution, consistent with progressive particle association/aggregation and increased heterogeneity of the dispersion.

The pronounced change in RZ-NPs may be associated with the intrinsic colloidal characteristics of zein. Zein is an amphiphilic protein containing a high proportion of hydrophobic amino acid residues, and exposed hydrophobic domains can promote intermolecular association in aqueous environments. During storage, close contact between unprotected zein nanoparticle surfaces may facilitate hydrophobic interactions together with other non-covalent attractive forces, promoting particle–particle association. Non-uniform aggregation can result in the coexistence of primary nanoparticles and aggregates of different sizes, which is consistent with the concurrent increase in mean hydrodynamic diameter and PDI observed for RZ-NPs.

In contrast, RZGG-NP showed considerably smaller changes during storage. The mean particle size increased from 165.4 to 178.6 nm, while the PDI changed only slightly from 0.164 to 0.175. This comparatively limited alteration is consistent with a stabilizing contribution from GG associated with the zein nanoparticle interface. The reversal of ζ-potential from +23.24 mV for RZ-NPs to −24.58 mV for RZGG-NP2:1 following GG incorporation supports substantial modification of the particle surface by the anionic polysaccharide. Surface-associated GG can provide a hydrated steric barrier around the nanoparticles, while simultaneously imparting negative surface charge. The resulting combination of steric hindrance and electrostatic repulsion can reduce close particle–particle contact and limit hydrophobic association between exposed zein domains, thereby reducing the propensity for aggregation.

After 30 days, the ζ-potential of RZGG-$NP_{2:1}$ changed from −24.58 to −20.39 mV, indicating some alteration in the interfacial properties during storage. Nevertheless, the relatively small changes in particle size and PDI suggest that extensive aggregation did not occur under the investigated conditions. Overall, the results indicate that GG association reduced the susceptibility of RSV-loaded zein nanoparticles to storage-induced aggregation and size-distribution broadening, consistent with an electrosteric stabilization effect.

The present findings also emphasize the importance of evaluating formulation stability using complementary physicochemical and performance-related parameters. Previous work has demonstrated that dissolution testing can reveal storage-induced changes in pharmaceutical performance that may not be fully apparent from drug-content determination or solid-state characterization alone.[51] Accordingly, while the comparatively small changes in particle size and PDI of RZGG-NPs provide encouraging evidence of improved short-term physical stability relative to uncoated RZ-NPs, comprehensive long-term stability studies incorporating drug content, physicochemical characteristics, and *in vitro* release behavior would be valuable for establishing the extended pharmaceutical stability of the developed formulation.[52]

CONCLUSION

In the present study, resveratrol-loaded zein–gum ghatti nanoparticles (RZGG-NPs) were successfully developed and characterized as a biopolymer-based delivery system for RSV. The optimized formulation exhibited favorable particle characteristics, high RSV encapsulation, and physicochemical features supporting successful incorporation of RSV within the zein–GG matrix. FTIR analysis indicated changes in the molecular environment of the formulation components consistent with non-covalent associations, while the complementary XRD and DSC findings demonstrated a pronounced reduction in the detectable crystalline order of RSV following nanoparticle formation.

The RZGG-NPs exhibited a distinct *in vitro* release profile under sequential simulated gastrointestinal conditions, with comparatively restricted RSV release during the gastric phase followed by progressive release under subsequent intestinal conditions. The formulation also retained the antioxidant activity of RSV in the DPPH assay. In COLO-205 cells, RZGG-NPs produced a concentration-dependent reduction in cell viability and showed greater cytotoxic activity than free RSV at corresponding concentrations under the investigated *in vitro* conditions. In addition, the comparatively limited changes in particle size and PDI of RZGG-NPs during the 30-day storage study suggested improved colloidal stabilization relative to uncoated RZ-NPs.

Collectively, these findings demonstrate the potential of the zein–GG nanoparticle platform for modulating the physicochemical characteristics and *in vitro* performance of RSV. The favorable release behavior and cytotoxic response observed in the present study provide a basis for further investigation of RZGG-NPs for oral RSV delivery. Future studies involving long-term stability assessment, cellular uptake and mechanistic investigations, *in vivo* pharmacokinetics, gastrointestinal distribution, biodistribution, antitumour efficacy, and safety evaluation will be necessary to determine whether the observed *in vitro* advantages translate into improved oral bioavailability and therapeutic performance *in vivo*.

ACKNOWLEDGMENT: The authors express their gratitude to the Principal and Management of the H. R. Patel Institute of Pharmaceutical Education and Research, Shirpur, for offering the necessary facilities.

REFERENCES

1 F. Acevedo, J. Hermosilla, C. Sanhueza, B. Mora-Lagos, I. Fuentes *et al*., *Eur. J. Pharm. Sci*., **119**, 49 (2018), https://doi.org/10.1016/j.ejps.2018.04.008

2 Z. Hatime, K. El Kinany, I. Huybrechts, N. Murphy, M. J. Gunter *et al*., *Asian Pac. J. Cancer Prev*., **23**, 1859 (2022)

3 S. Shinde, V. Sinha, V. Dixit, M. Dwivedi, N. K. Vishwakarma *et al*., "Colon Cancer Diagnosis and Therapy", vol. 2, Springer, 2021, pp. 15-52

4 B. A. Carneiro and W. S. El-Deiry, *Nat. Rev. Clin. Oncol*., **17**, 395 (2020)

5 S. Goldar, M. S. Khaniani, S. M. Derakhshan and B. Baradaran, *Asian Pac. J. Cancer Prev*., **16**, 2129 (2015)

6 M. Hassan, H. Watari, A. A. Almaaty, Y. Ohba and N. Sakuragi, *Biomed Res. Int*., **2014**, 2451249 (2020)

7 G. Pistritto, D. Trisciuoglio, C. Ceci, A. Garufi and G. D'Orazi, *Aging*, **8**, 603 (2016)

8 M. M. Atakan, Ş. N. Koşar, Y. Güzel, H. T. Tin and X. Yan, *Nutrients*, **13**, 1459 (2021), https://doi.org/10.3390/nu13051459

9 D. Delmas, V. Aires, E. Limagne, P. Dutartre, F. Mazué *et al*., *Ann. N. Y. Acad. Sci*., **1215**, 48 (2011), https://doi.org/10.1111/j.1749-6632.2010.05871.x

[10] A. Lasa, I. Churruca, I. Eseberri, C. Andrés-Lacueva and M. P. Portillo, *Mol. Nutr. Food Res.*, **56**, 1559 (2012), https://doi.org/10.1002/mnfr.201200128
[11] E. Polycarpou, L. B. Meira, S. Carrington, E. Tyrrell, H. Modjtahedi *et al.*, *Mol. Nutr. Food Res.*, **57**, 1708 (2013), https://doi.org/10.1002/mnfr.201200842
[12] Chimento, F. De Amicis, R. Sirianni, M. S. Sinicropi, F. Puoci *et al.*, *Int. J. Mol. Sci.*, **20**, 1381 (2019), https://doi.org/10.3390/ijms20061381
[13] N. Summerlin, E. Soo, S. Thakur, Z. Qu, S. Jambhrunkar *et al.*, *Int. J. Pharm.*, **479**, 282 (2015), https://doi.org/10.1016/j.ijpharm.2015.01.003
[14] M. A. Augustin, L. Sanguansri and T. Lockett, *Ann. N. Y. Acad. Sci.*, **1290**, 107 (2013), https://doi.org/10.1111/nyas.12138
[15] M. Krstić, Z. Maksimović, S. Ibrić, T. Bakić, J. Prodanović *et al.*, *Cellulose Chem. Technol.*, **52**, 577 (2018), https://www.cellulosechemtechnol.ro/pdf/CCT7-8(2018)/p.577-588.pdf
[16] I. J. Joye, G. Davidov-Pardo and D. J. McClements, *Food Hydrocoll.*, **49**, 127 (2015), https://doi.org/10.1016/j.foodhyd.2015.03.009
[17] T. Saha, M. E. Hoque and T. Mahbub, "Advanced Processing, Properties, and Applications of Starch and Other Bio-Based Polymers", Elsevier, 2020, pp. 197-214
[18] Y. Zhang, L. Cui, F. Li, N. Shi, C. Li *et al.*, *Int. J. Pharm.*, **513**, 191 (2016), https://doi.org/10.1016/j.ijpharm.2016.09.017
[19] Q. Zhong and M. Jin, *Food Hydrocoll.*, **23**, 2380 (2009), https://doi.org/10.1016/j.foodhyd.2009.06.015
[20] X. Wang and X. Chu, *Colloids Surf. A Physicochem. Eng. Asp.*, **558**, 110 (2018), https://doi.org/10.1016/j.colsurfa.2018.08.070
[21] A. R. Patel, E. C. Bouwens and K. P. Velikov, *J. Agric. Food Chem.*, **58**, 12497 (2010), https://doi.org/10.1021/jf102959p
[22] S. Chen, Q. Li, D. J. McClements, Y. Han, L. Dai *et al.*, *Food Hydrocoll.*, **99**, 105334 (2020), https://doi.org/10.1016/j.foodhyd.2019.105334
[23] K. Yao, W. Chen, F. Song, D. J. McClements and K. Hu, *Food Hydrocoll.*, **79**, 262 (2018), https://doi.org/10.1016/j.foodhyd.2017.12.035
[24] M. Shaikh, N. Desai, M. Momin and L. K. Bhatt, *Curr. Drug Deliv.*, **18**, 1563 (2021)
[25] A. J. Kora, S. R. Beedu and A. Jayaraman, *Org. Med. Chem. Lett.*, **2**, 17 (2012), https://doi.org/10.1186/2191-2858-2-17
[26] P. Pal, S. K. Singh, S. Mishra, J. P. Pandey and G. Sen, *Carbohyd. Polym.*, **222**, 114979 (2019), https://doi.org/10.1016/j.carbpol.2019.114979
[27] P. Sapale, V. Bhadariya, S. S. Rana, T. Subbaiah, M. V. Chavhan *et al.*, *Petroleum*, **8**, 567 (2022), https://doi.org/10.1016/j.petlm.2021.10.006
[28] D. Sinha, S. Seth, A. Das, U. K. Bhattacharyya, K. Ghosh *et al.*, *J. Drug Deliv. Sci. Technol.*, **76**, 103730 (2022), https://doi.org/10.1016/j.jddst.2022.103730
[29] X. Huang, Y. Dai, J. Cai, N. Zhong, H. Xiao *et al.*, *Food Hydrocoll.*, **64**, 157 (2017), https://doi.org/10.1016/j.foodhyd.2016.10.029
[30] Y. Wei, C. Sun, L. Dai, X. Zhan and Y. Gao, *Food Hydrocoll.*, **81**, 149 (2018), https://doi.org/10.1016/j.foodhyd.2018.02.036.
[31] X. Wang, H. Gu, H. Zhang, J. Xian, J. Li *et al.*, *ACS Appl. Mater. Interfaces*, **13**, 33948 (2021), https://doi.org/10.1021/acsami.1c07162
[32] X. Huang, Y. Liu, Y. Zou, X. Liang, Y. Peng *et al.*, *Food Hydrocoll.*, **93**, 261 (2019), https://doi.org/10.1016/j.foodhyd.2019.02.020
[33] K. Hu and D. J. McClements, *Food Hydrocoll.*, **44**, 101 (2015), https://doi.org/10.1016/j.foodhyd.2014.08.018
[34] Y. Luo, Z. Teng and Q. Wang, *J. Agric. Food Chem.*, **60**, 836 (2012), https://doi.org/10.1021/jf204194z
[35] D. J. McClements, "Food Emulsions: Principles, Practices, and Techniques", CRC Press, Boca Raton, 2004
[36] Q. Liu, Y. Qin, B. Jiang, J. Chen and T. Zhang, *Colloids Surf. B Biointerfaces*, **216**, 112529 (2022), https://doi.org/10.1016/j.colsurfb.2022.112529
[37] R. Shukla and M. Cheryan, *Ind. Crop. Prod.*, **13**, 171 (2001), https://doi.org/10.1016/S0926-6690(00)00064-9
[38] C. Chang, T. Wang, Q. Hu, M. Zhou, J. Xue *et al.*, *Food Hydrocoll.*, **70**, 143 (2017), https://doi.org/10.1016/j.foodhyd.2017.03.017
[39] H. Liang, B. Zhou, J. Li, Y. He, Y. Pei *et al.*, *RSC Adv.*, **6**, 101267 (2016), https://doi.org/10.1039/C6RA21300H
[40] G. Babaladimath, *J. Polym. Res.*, **24**, 155 (2017), https://doi.org/10.1007/s10965-017-1312-0
[41] X. Ren, T. Hou, Q. Liang, X. Zhang, D. Hu *et al.*, *Food Chem.*, **279**, 223 (2019), https://doi.org/10.1016/j.foodchem.2018.11.126
[42] R. Sun, G. Zhao, S. Ni and Q. Xia, *J. Drug Deliv. Sci. Technol.*, **24**, 591 (2014)
[43] P. H. Tran, W. Duan, B.-J. Lee and T. T. Tran, *Int. J. Pharm.*, **569**, 118614 (2019), https://doi.org/10.1016/j.ijpharm.2019.118614
[44] A. T. Mneimneh, B. Hayar, S. Al Hadeethi, N. Darwiche and M. M. Mehanna, *Int. J. Biol. Macromol.*, **281**, 136437 (2024), https://doi.org/10.1016/j.ijbiomac.2024.136437
[45] W. Wang, Y. Cui, H. Zhao, L. Jia, X. Ding *et al.*, *Food Res. Int.*, **214**, 116656 (2025), https://doi.org/10.1016/j.foodres.2025.116656
[46] G. Navarro, E. Martínez-Pinilla, R. Ortiz, V. Noé, C. J. Ciudad *et al.*, *Compr. Rev. Food Sci. Food Saf.*, **17**, 808 (2018), https://doi.org/10.1111/1541-4337.12359
[47] J. A. Tapia-Hernández, F. Rodríguez-Felix, J. E. Juárez-Onofre, S. Ruiz-Cruz, M. A. Robles-García *et al.*, *Food Res. Int.*, **111**, 451 (2018), https://doi.org/10.1016/j.foodres.2018.05.036
[48] H. J. Freeman, *World J. Gastroenterol.*, **19**, 8468 (2013), https://doi.org/10.3748/wjg.v19.i46.8468

[49] G. Mazzone, N. Malaj, N. Russo and M. Toscano, *Food Chem*., **141**, 2017 (2013), https://doi.org/10.1016/j.foodchem.2013.05.050
[50] A. R. Neves, S. Martins, M. A. Segundo and S. Reis, *Nutrients*, **8**, 131 (2016), https://doi.org/10.3390/nu8030131
[51] F. Ma, W. Lv, L. Wu, C. Duan, X. Li *et al*., *Food Biosci*., **68**, 106664 (2025), https://doi.org/10.1016/j.fbio.2025.106664
[52] E. Osmanović Omerdić, L. Alagić-Džambić, M. Krstić, M. Pašić-Kulenović, Đ. Medarević *et al*., *PLoS ONE*, **17**, e0266237 (2022), https://doi.org/10.1371/journal.pone.0266237